

**Isoscalar giant monopole resonance in Sn isotopes using a quantum molecular dynamics model**C. Tao (陶城),<sup>1,\*</sup> Y. G. Ma (马余刚),<sup>1,2,†</sup> G. Q. Zhang (张国强),<sup>1</sup> X. G. Cao (曹喜光),<sup>1,2</sup> D. Q. Fang (方德清),<sup>1,2</sup> H. W. Wang (王宏伟),<sup>1</sup> and J. Xu (徐骏)<sup>1</sup><sup>1</sup>Shanghai Institute of Applied Physics, Chinese Academy of Sciences, Shanghai 201800, China<sup>2</sup>Kavli Institute for Theoretical Physics, Chinese Academy of Sciences, Beijing 100190, China

(Received 26 July 2013; revised manuscript received 1 December 2013; published 30 December 2013)

The isoscalar giant monopole resonance (GMR) in Sn isotopes and other nuclei is investigated in the framework of the isospin-dependent quantum molecular dynamics (IQMD) model. The spectrum of GMR is calculated by taking the rms radius of a nucleus as its monopole moment. The peak energy, the FWHM, and the strength of the GMR extracted by a Gaussian fit to the spectrum have been studied. The GMR peak energies for Sn isotopes from the calculations using a mass-number-dependent Gaussian wave-packet width  $\sigma_r$  for nucleons are found to be overestimated and show a weak dependence on the mass number compared with the experimental data. However, it is found that experimental data of the GMR peak energies for <sup>56</sup>Ni, <sup>90</sup>Zr, and <sup>208</sup>Pb as well as Sn isotopes can be nicely reproduced after taking into account the isospin dependence in isotope chains in addition to the mass-number dependence of  $\sigma_r$  for nucleons in the IQMD model calculation.

DOI: 10.1103/PhysRevC.88.064615

PACS number(s): 24.30.Cz, 25.70.Ef, 21.65.Ef, 24.10.Lx

**I. INTRODUCTION**

The isoscalar giant monopole resonance (GMR), known as the so-called breathing mode, is one of the collective modes of nuclei. In the past decades, GMR was extensively studied both theoretically [1–10] and experimentally [11–15]. Especially, a strong correlation between the peak energy of GMR and the nuclear incompressibility  $K_0$  at the nuclear saturation density was found [16]. The studies from both relativistic and nonrelativistic models have reached a consensus on the value of the nuclear incompressibility at  $K_0 \sim 240 \pm 10$  MeV [2–4].

Recently, GMR along the Sn isotopic chain was studied experimentally [12–14]. From the analysis based on the GMR data for Sn isotopes, the asymmetry term of the nuclear incompressibility was constrained, i.e.,  $K_\tau \sim -550 \pm 100$  MeV [12]. Similar analysis on the GMR data in the Cd isotopes gave a preliminary value of  $K_\tau \sim -555 \pm 75$  MeV [17]. Comparison between the experimental data and the theoretical results has indicated that models which can reproduce the peak energies of GMR in <sup>90</sup>Zr, <sup>144</sup>Sm, and <sup>208</sup>Pb overestimate those in Sn isotopes. This realization leaves a puzzling question: Why is tin so soft? [5]. In Ref. [1], the effect of pairing correlations on the peak energy of GMR was considered. However, the result that the peak energies of GMR in Sn isotopes are shifted by about 100–150 keV compared to the case without pairing correlations was insufficient to explain the experimental data. In Ref. [6], a hybrid model with a small nuclear incompressibility of  $K_0 = 230$  MeV as FSUGold and a stiff symmetry energy as NL3 was built. Although the improvement in the description for the experimental data of Sn isotopes was significant and unquestionable, the hybrid model still underestimated the peak energy of GMR in <sup>208</sup>Pb by almost 1 MeV. The authors of Ref. [6] also suggested that the rapid softening with neutron excess predicted by the hybrid

model might be unrealistic. More details of the discussion on this anomaly can be found in Refs. [1,6–9,14].

In the previous works, our group applied the isospin-dependent quantum molecular dynamics (IQMD) model to study the dynamical dipole emission in fusion reactions [18] and giant dipole resonances (GDRs) as well as pygmy dipole resonances (PDRs) in Ni isotopes by Coulomb excitations [19]. In the present work, we will investigate GMR in Sn isotopes within a similar framework. We will show that using a new function of the Gaussian wave-packet width, which takes the isospin dependence into account, we are able to reproduce very well the GMR peak energies for <sup>56</sup>Ni, <sup>90</sup>Zr, and <sup>208</sup>Pb as well as Sn isotopes.

The paper is organized as follows. Section II gives a brief introduction of the IQMD model as well as the formalism for GMR in the IQMD framework. Results and discussions are presented in Sec. III, where effects from the impact parameter, incident energy, equation of state (EOS), symmetry energy, and width of the Gaussian wave packet used in the IQMD model on GMR are investigated. A summary is given in Sec. IV.

**II. MODEL AND FORMALISM****A. Brief description of IQMD model**

The IQMD model, which is based on the QMD model, is a kind of Monte Carlo transport model [20–26]. The wave function of each nucleon is represented by a Gaussian form:

$$\phi_i(\vec{r}, t) = \frac{1}{(2\pi L)^{3/4}} \exp \left[ -\frac{[\vec{r} - \vec{r}_i(t)]^2}{(2\sigma_r)^2} - \frac{i\vec{r} \cdot \vec{p}_i(t)}{\hbar} \right]. \quad (1)$$

In the above,  $\sigma_r$  is the width parameter for the Gaussian wave packet, and its value depends on the size of the reacting system to keep some quantum effect of nucleons. We will see in the following that the influence of the width on GMR should be treated carefully to reproduce the experimental results.  $\vec{r}_i(t)$  and  $\vec{p}_i(t)$  are the position and momentum coordinates of the  $i$ th nucleon. After performing the variation method, the equations of motion, i.e., the time evolution of the mean position  $\vec{r}_i(t)$

\*Present address: Shandong Tumor Hospital, Jinan 250117, China.

†Corresponding author: ygma@sinap.ac.cn

and momentum  $\vec{p}_i(t)$ , are found to be

$$\dot{\vec{p}}_i = -\frac{\partial \langle H \rangle}{\partial \vec{r}_i} \quad \text{and} \quad \dot{\vec{r}}_i = \frac{\partial \langle H \rangle}{\partial \vec{p}_i}. \quad (2)$$

$\langle H \rangle$  is the total Hamiltonian of the system

$$\langle H \rangle = \langle T \rangle + \langle V \rangle, \quad (3)$$

where the  $\langle T \rangle$  is the kinetic contribution, and  $\langle V \rangle$  is the potential contribution

$$\langle V \rangle = \frac{1}{2} \sum_i \sum_{j \neq i} \int f_i(\vec{r}, \vec{p}, t) V^{ij} f_j(\vec{r}', \vec{p}', t) d\vec{r} d\vec{r}' d\vec{p} d\vec{p}'. \quad (4)$$

In the above, the Wigner distribution function  $f_i(\vec{r}, \vec{p}, t)$ , which is the phase-space density of the  $i$ th nucleon, is obtained by applying the Wigner transformation on the single nucleon wave function

$$f_i(\vec{r}, \vec{p}, t) = \frac{1}{\pi^3 \hbar^3} \exp \left[ -\frac{[\vec{r} - \vec{r}_i(t)]^2}{2\sigma_r^2} - \frac{2\sigma_r^2[\vec{p} - \vec{p}_i(t)]^2}{\hbar^2} \right], \quad (5)$$

and  $V^{ij}$  is the two-body interaction including the contact Skyrme-type interaction, the finite-range Yukawa potential, the momentum-dependent interaction (MDI), the isospin-dependent interaction, and the Coulomb interaction

$$\begin{aligned} V^{ij} &= V_{\text{Skyrme}}^{ij} + V_{\text{Yuk}}^{ij} + V_{\text{asy}}^{ij} + V_{\text{MDI}}^{ij} + V_{\text{Coul}}^{ij} \\ &= t_1 \delta(\vec{r} - \vec{r}') + t_2 \rho^{\sigma-1}(\vec{r}) \delta(\vec{r} - \vec{r}') \\ &\quad + t_3 \frac{\exp[-|\vec{r} - \vec{r}'|/\mu]}{|\vec{r} - \vec{r}'|/\mu} + t_6 \rho^{\gamma-1}(\vec{r}) T_{3i} T_{3j} \delta(\vec{r} - \vec{r}') \\ &\quad + t_4 \ln^2[1 + t_5(\vec{p} - \vec{p}')^2] \delta(\vec{r} - \vec{r}') + \frac{Z_i Z_j e^2}{|\vec{r} - \vec{r}'|}, \end{aligned} \quad (6)$$

where  $Z$  is the charge of the nucleon, and  $t_1, \dots, t_6$  and  $\mu$  are the parameters to fit the empirical properties of nuclear matter as well as nuclei.

In the following, we will give the expressions for the Skyrme potential, the momentum-dependent potential, and the symmetry potential to ease discussions for the GMR results. The Skyrme potential is

$$U_{\text{Sky}} = \alpha u + \beta u^\sigma, \quad (7)$$

where  $u = \rho_{\text{int}}/\rho_0$  is the reduced density with  $\rho_0 = 0.16 \text{ fm}^{-3}$  being the nuclear saturation density and  $\rho_{\text{int}} = \sum \rho_{\text{int}}^i(\vec{r})$  with

$$\rho_{\text{int}}^i(\vec{r}) = \frac{1}{(4\pi\sigma_r^2)^{3/2}} \sum_{j \neq i} e^{-(\vec{r}-\vec{r}_j)^2/(4\sigma_r^2)} \quad (8)$$

being the interaction density of the  $i$ th nucleon. We will in the following denote  $\rho_{\text{int}}$  as  $\rho$  for simplicity.  $\alpha$ ,  $\beta$ , and  $\sigma$  are the Skyrme parameters related to the isoscalar EOS of bulk nuclear matter. The momentum-dependent potential, which is optional in the IQMD model, can be expressed as

$$U_{\text{MDI}} = \frac{\rho_{\text{int}}}{\rho_0} \int d\vec{p}' g_j(\vec{p}', t) \delta \ln^2[\epsilon(\vec{p} - \vec{p}')^2 + 1], \quad (9)$$

TABLE I. Parameters  $\alpha$ ,  $\beta$ , and  $\sigma$  for different EOSs.

	$K_0$ (MeV)	$\alpha$ (MeV)	$\beta$ (MeV)	$\sigma$
Soft	200	-356	303	7/6
Soft+MDI	200	-390.1	320.3	1.14
Hard	380	-124	70.5	2
Hard+MDI	380	-129.2	59.4	2.09

where  $g_j(\vec{p}, t) = \frac{1}{(\pi\hbar)^{3/2}} \exp[-\frac{2\sigma_r^2(\vec{p}-\vec{p}_j(t))^2}{\hbar^2}]$  is the momentum density distribution function of nucleon, and  $\delta = 1.57 \text{ MeV}$  and  $\epsilon = 500 (\text{GeV}/c)^{-2}$  are taken from the measured energy dependence of the proton-nucleus optical potential [20–24]. The isospin asymmetry potential can be also calculated from Eq. (4) as

$$U_{\text{sym}} = \frac{C_{\text{sym}}}{2} [(\gamma - 1)u^\gamma \delta^2 \pm 2u^\gamma \delta], \quad (10)$$

where  $\delta = (\rho_n - \rho_p)/\rho$  is the local isospin asymmetry from the contribution of all the other nucleons, and the symbol  $+$  ( $-$ ) is for neutrons (protons),  $\gamma$  is the stiffness parameter of the symmetry potential (energy), and  $C_{\text{sym}}$  is the potential contribution of the symmetry energy at saturation density.

The nuclear incompressibility is calculated from the second-order derivative of the binding energy per nucleon as

$$K_0 = 9\rho_0^2 \frac{\partial^2}{\partial \rho^2} \left( \frac{E}{A} \right)_{\rho=\rho_0}. \quad (11)$$

Table I gives different parameter sets for the Skyrme potential with and without the momentum-dependent potential, leading to the nuclear incompressibility of 200 and 380 MeV. As mentioned in the Introduction, although the latest experimental analysis leads to  $K_0 \approx 240 \text{ MeV}$ , we will use these extreme values to illustrate the sensitivity of the GMR peak energy on the nuclear incompressibility as well as the momentum dependence of the nuclear potential based on the IQMD model.

## B. Calculation method of giant monopole resonance

In the present framework, we first pick up a stable initial density distribution for a concerned nucleus, e.g.,  $^{112}\text{Sn}$ , as is done for most QMD model studies. This density distribution is generally not the ground state for the nuclear interaction used, so the nucleus suffers from collective oscillation in its excited state [28], among them is the GMR mode. As GMR is a compression mode in the radial direction, we take the rms radius of the nucleus as its monopole moment  $D_{\text{GMR}}(t)$  at each time step [27,28], as is shown by the solid line in Fig. 1. One sees that the rms radius shows good oscillation structure, i.e., the GMR mode. However, the oscillation damps quickly due to the dissipation effect from both the mean-field potential and the nucleon-nucleon scatterings [28]. It is noteworthy that the period and the decay of the GMR oscillation leads respectively to the peak energy and the width of the GMR spectrum, which can still be hardly reproduced simultaneously [28]. In the present study, we use  $^{208}\text{Pb}$  as a target and the concerned nucleus as the projectile. In this way, the strength, period,

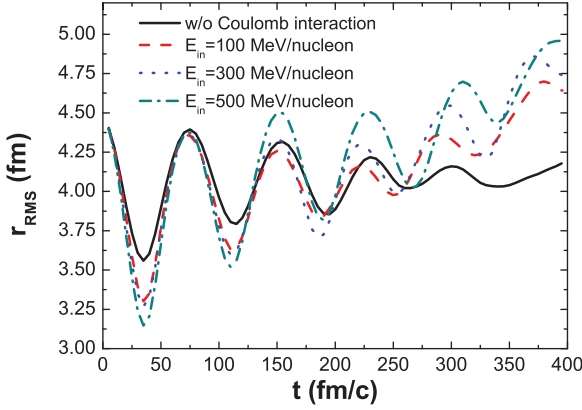


FIG. 1. (Color online) Time evolution of the calculated rms radius of  $^{112}\text{Sn}$  without Coulomb interaction and reacting on the  $^{208}\text{Pb}$  target at different beam energies of 100, 300, and 500 MeV/nucleon, respectively, with impact parameter of 30 fm.

and damping of the GMR oscillation are thus modified by the Coulomb interaction between the projectile and the target, as shown in Fig. 1. It is seen that with Coulomb interaction, the rms radii have a larger amplitude and a little longer oscillation period with the increasing of the beam energy and become larger on average in the later stage. Overall, a good oscillation behavior of the rms radius in a relative long time scale is the key to forming a GMR mode. Of course, considering the stability of time evolution of the rms radius in the present model, we calculate the GMR spectra by 200 fm/c.

By applying the Fourier transformation to the second-order derivative of  $D_{\text{GMR}}(t)$  with respect to time

$$D''(\omega) = \int_{t_0}^{t_{\text{max}}} D''_{\text{GMR}}(t) e^{i\omega t} dt, \quad (12)$$

one can get the spectrum of probability for energy  $E_\gamma = \hbar\omega$  as follows

$$\frac{dP}{dE_\gamma} = \frac{2e^2}{3\pi\hbar c^3 E_\gamma} |D''(\omega)|^2. \quad (13)$$

As mentioned above, we set the stopping time of the monopole moment ( $t_{\text{max}}$ ) as 200 fm/c in the present calculation. From a Gaussian fit to the spectrum of GMR, one can get the peak energy  $E_\gamma^c$ , the FWHM  $\Gamma_\gamma^c$ , and the strength  $S_\gamma^c$  of GMR.

### III. RESULTS AND DISCUSSIONS

#### A. GMR spectrum comparison

The GMR spectra for  $^{112}\text{Sn}$  and  $^{124}\text{Sn}$  from our calculations are compared with the experimental data from Ref. [12] in Fig. 2. Note that there is one major different point which we should mention in this comparison between our calculation and the data. In Ref. [12], the GMR data are taken from the excited Sn nucleus by inelastic scattering of 400-MeV  $\alpha$  particles at extremely forward angles. However, in our calculation, the GMR comes from the excited oscillation of the Sn nucleus, because the initial density distribution is not the ground state of the nuclear interaction used. The reason is based on the following consideration: (1) it is not an easy

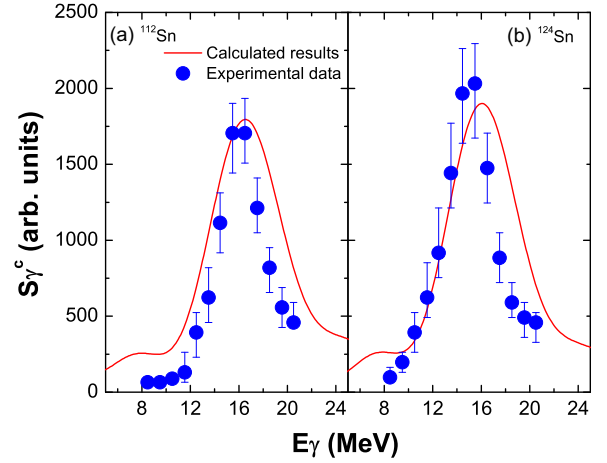


FIG. 2. (Color online) Calculated results of GMR in  $^{112}\text{Sn}$  and  $^{124}\text{Sn}$  compared with the experimental data. Note that the condition to induce the GMR is different for the experimental data and the present calculation (see texts for more details). The blue circles with error bars are the experimental data from inelastic scattering [12], and the red line is the result from the IQMD calculation.

task to treat inelastic scattering of  $\alpha$  particles in our IQMD model even though the data are available; (2) the peak energy and the FWHM are determined by the intrinsic properties of the nucleus and independent of how the GMR mode is excited. Consequently, we have to take a compromise for the comparison, i.e., taking the GMR for the same excited nucleus but with a different reaction mechanism, with the strength  $S_\gamma^c$  of GMR from our calculation scaled by that from the experimental data. In this background, we introduce the parameters used in our calculations as follows: incident energy  $E_{\text{in}} = 386$  MeV/nucleon, impact parameter  $b = 30$  fm, the soft EOS with MDI,  $C_{\text{sym}} = 35.2$  MeV, and  $\gamma = 1$ . Although the condition of our calculation is different from that of the experiment in Ref. [12] as mentioned above, one can see that our results from the oscillation of excited nuclei modified by the Coulomb interaction show a reasonable agreement with the inelastic  $\alpha$  scattering experimental data, i.e., giving a similar peak energy but a slightly larger FWHM. The calculated result of  $^{112}\text{Sn}$  shows a better agreement with the experimental data than that of  $^{124}\text{Sn}$ . The results indicate that the IQMD model is suitable for the study of GMR by considering the rms radius as its monopole moment.

#### B. Systematic GMR analysis

The sensitivities of the peak energy, the FWHM, and the strength obtained by a Gaussian fit to the GMR spectrum have been explored. The sensitivity of these quantities to the impact parameter for  $^{112}\text{Sn}$  is given in Fig. 3. It shows that the GMR results do not change much with the increasing impact parameter. This is understandable since the effect of the Coulomb interaction is not affected by much when the impact parameter changes from 25 to 40 fm. Figure 4 shows the incident energy dependence of GMR results for  $^{112}\text{Sn}$ . With the increase of the incident energy, the peak energy of GMR decreases, while the FWHM and the strength of GMR

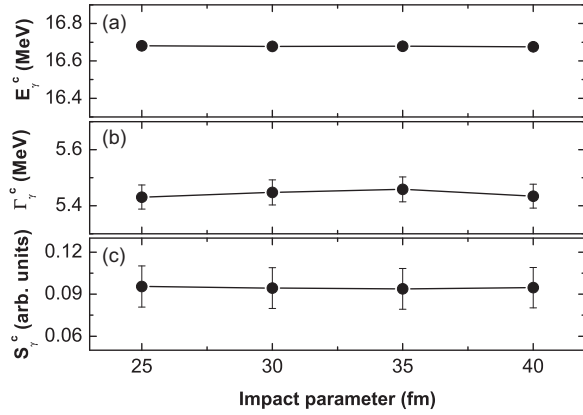


FIG. 3. Impact parameter dependence of the peak energy  $E_\gamma^c$ , the FWHM  $\Gamma_\gamma^c$ , and the strength  $S_\gamma^c$  of GMR for  $^{112}\text{Sn}$ . In the calculation, we use  $E_{\text{in}} = 386$  MeV/nucleon,  $C_{\text{sym}} = 35.2$  MeV,  $\gamma = 1$ , and the soft EOS with MDI.

increase. This behavior can be understood by the oscillation of rms radii at different beam energies as shown in Fig. 1. As we know, the longer oscillation period corresponds to the lower frequency, i.e., lower energy, while the higher amplitude corresponds to the larger strength. Figure 1 tells us that with the increasing beam energy, the GMR monopole moment has a little longer period but a larger amplitude, which results in a decreasing peak energy and an increasing strength of GMR as shown in Fig. 4. From the above discussions, it is seen that although the GMR oscillation is already there for a nucleus alone, it can be slightly modified by the Coulomb interaction with different incident energies and impact parameters.

Many previous works indicated that the EOS associated with the nuclear incompressibility  $K_0$  has an important influence on GMR, i.e., the peak energy of GMR can be used to constrain  $K_0$ . By adjusting the parameters of EOS in Table I used in the IQMD model, the EOS dependence of GMR parameters for  $^{112}\text{Sn}$  can be explored. The sensitivity of the GMR results to the EOS are illustrated in Fig. 5, where a significant dependence of the GMR peak energy on the EOS can be seen. In general, the hard EOS gives a higher peak

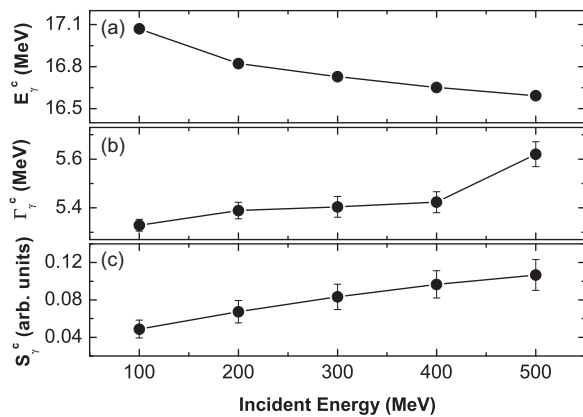


FIG. 4. Same as Fig. 3, but for the incident energy dependence of the GMR results for  $^{112}\text{Sn}$ . In the calculation, we use  $b = 30$  fm,  $C_{\text{sym}} = 35.2$  MeV,  $\gamma = 1$ , and the soft EOS with MDI.

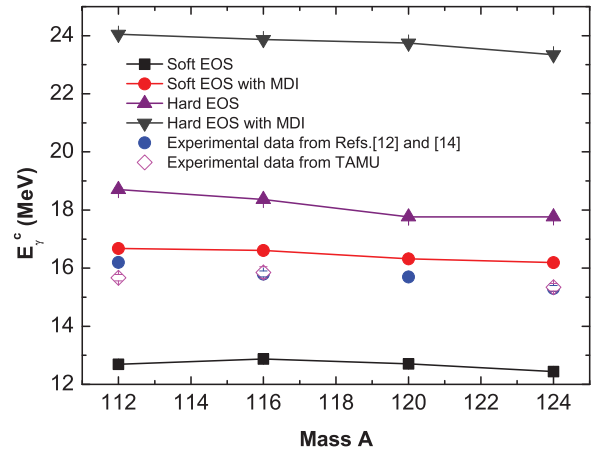


FIG. 5. (Color online) Peak energies of GMR in Sn isotopes when different EOS parameters are used. In the calculation, we use  $E_{\text{in}} = 386$  MeV/nucleon,  $b = 30$  fm,  $C_{\text{sym}} = 35.2$  MeV, and  $\gamma = 1$ . The blue circles with error bar are the experimental data from Refs. [12,14], and the open diamonds with error bar are the experimental data from Refs. [29,30].

energy than the soft one, and so does the EOS with MDI. In this sense, a soft EOS with MDI can reproduce the results from a hard EOS without MDI. Similar results on giant or pygmy dipole resonances are seen within the same model [19]. By comparing the calculated results with the experimental data [12,29,30], one can see that the soft EOS with MDI shows the best agreement with the experimental data.

The GMR results may also be affected by the nuclear symmetry energy which is important in understanding the structure of neutron- or proton-rich nuclei and the reaction dynamics of heavy-ion collisions [31,32]. Again we use the extreme values of  $C_{\text{sym}}$  and  $\gamma$  to illustrate the sensitivity of the GMR results to the nuclear symmetry energy. The dependence of the GMR results on the parameter  $C_{\text{sym}}$  is shown in Fig. 6. When  $C_{\text{sym}}$  changes from 16 to 64 MeV, the peak energy of GMR shows a decreasing behavior, the FWHM of GMR increases, and the strength of GMR slightly decreases. The  $\gamma$  dependence of the GMR results is shown in Fig. 7. When

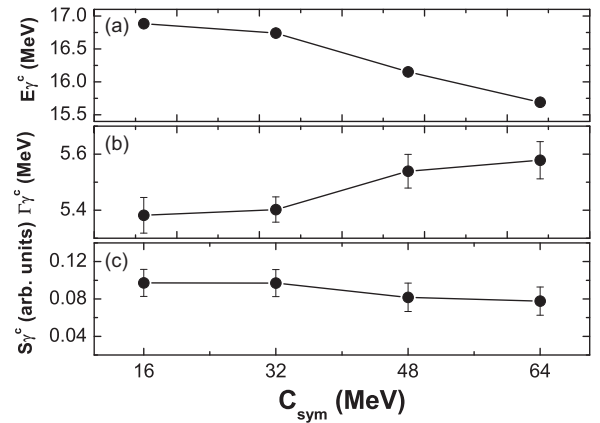


FIG. 6. Same as Fig. 3, but for  $C_{\text{sym}}$  dependence of GMR results for  $^{112}\text{Sn}$ . In the calculation, we use  $E_{\text{in}} = 386$  MeV/nucleon,  $b = 30$  fm,  $\gamma = 1$ , and the soft EOS with MDI.

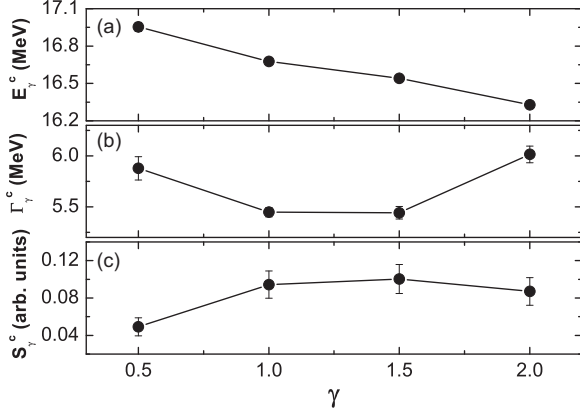


FIG. 7. Same as Fig. 3, but for the  $\gamma$  dependence of GMR results for  $^{112}\text{Sn}$ . In the calculation, we use  $E_{\text{in}} = 386$  MeV/nucleon,  $b = 30$  fm,  $C_{\text{sym}} = 35.2$  MeV, and the soft EOS with MDI.

$\gamma$  changes from 0.5 to 2, the peak energy of GMR also decreases, while the FWHM and the strength of GMR show a nonmonotonical behavior. To understand the dependence of the GMR peak energy on the symmetry energy, we express it in the form of [33]

$$E_\gamma^c = \hbar \sqrt{\frac{K_A}{m \langle r^2 \rangle}}, \quad (14)$$

where  $m$  is the nucleon mass,  $\langle r^2 \rangle$  is the ground state mean-square radius, and  $K_A$ , which is the incompressibility of a nucleus with mass  $A$ , can be written as [12]

$$K_A \sim K_V(1 + c_V A^{-1/3}) + K_\tau[(N - Z)/A]^2 + K_C Z^2 A^{-4/3}, \quad (15)$$

with  $N$  and  $Z$  the neutron and proton number, and  $K_V$  as well as  $c_V$ ,  $K_\tau$ , and  $K_C$  the coefficients for the volume, asymmetry, and Coulomb contributions, respectively. In the analysis of the symmetry energy effects on the GMR results where all the other parameters have been fixed,  $K_A$  increases with the increasing asymmetry incompressibility  $K_\tau$ , with the latter expressed as [34]

$$K_\tau = K_{\text{sym}} - 6L_s - \frac{J_0}{K_0} L_s. \quad (16)$$

The slope parameter  $L_s$  and the curve parameter  $K_{\text{sym}}$  at saturation density can be calculated from the expression of the symmetry energy as

$$L_s = 25 + \frac{3}{2} C_{\text{sym}} \gamma (\text{MeV}), \quad (17)$$

$$K_{\text{sym}} = -25 + \frac{9}{2} C_{\text{sym}} \gamma (\gamma - 1) (\text{MeV}).$$

$K_0$  and  $J_0$  are related to the isoscalar part of the equation of state  $E_0(\rho)$  in the form of

$$K_0 = 9\rho_0^2 \left( \frac{d^2 E_0}{d\rho^2} \right)_{\rho=\rho_0}, \quad (18)$$

$$J_0 = 27\rho_0^3 \left( \frac{d^3 E_0}{d\rho^3} \right)_{\rho=\rho_0}. \quad (19)$$

The dependence of  $E_\gamma^c$  on  $C_{\text{sym}}$  and  $\gamma$  in Figs. 6 and 7 can be understood from the above formulas.

The Gaussian wave-packet width  $\sigma_r$  [in Eq. (1)] for nucleons is a parameter in the IQMD model indicating the interaction range between nucleons. Previous studies have shown that the value  $\sigma_r$  has a large effect on GMR results [35]. In many previous QMD model calculations,  $\sigma_r$  is set to be a constant. However, there were also some discussions related to the influence of  $\sigma_r$  on the dynamical results, e.g., flow, multifragmentation, and pion and kaon production, etc. [21,36–40]. Since in a finite system nucleons are localized within a potential well, it is reasonable to make  $\sigma_r$  related to the size of a nucleus. For example, the width of the Gaussian wave packet is taken to be  $\sigma_r = 1.04$  fm for the Ca+Ca system and  $\sigma_r = 1.47$  fm for the Au+Au system in Ref. [21], while a system-size-dependent  $\sigma_r$  was presented in Ref. [40]. Actually, in some models like an extended quantum molecular dynamics (EQMD) model [37] and a fermionic molecular dynamics (FMD) model [38,39],  $\sigma_r$  is treated as a dynamical variable. In our IQMD model, we use a similar mass-number dependence of  $\sigma_r$  as in Ref. [40],

$$\sigma_r = 0.17A^{1/3} + 0.48(\text{fm}), \quad (20)$$

where  $A$  is the mass number of the system (projectile, target, or compound system). In heavy-ion reactions,  $\sigma_r$  for the compound system is set to be the mean value of that for the projectile and the target given by Eq. (20). In the present study, we just use  $\sigma_r$  for the concerned nucleus, i.e., the projectile. This is similar to the treatment in Ref. [40], where the projectile and target have their own  $\sigma_r$  before they contact in the heavy-ion reaction process, and after the contact, the projectile and the target gradually melt into one system, and consequently all the particles have a universal  $\sigma_r$ . Figure 8 displays the  $\sigma_r$  dependence of the GMR results. As  $\sigma_r$  increases, the peak energy and the FWHM of GMR show a clear decreasing trend, while the strength of GMR is not largely affected.

The influence of different forms of  $\sigma_r$  on the peak energy of GMR has also been studied. Figure 9 shows the calculated peak energies of GMR in Sn isotopes with the fixed  $\sigma_r = 1.47$  fm or the variational  $\sigma_r$  given by Eq. (20) together with

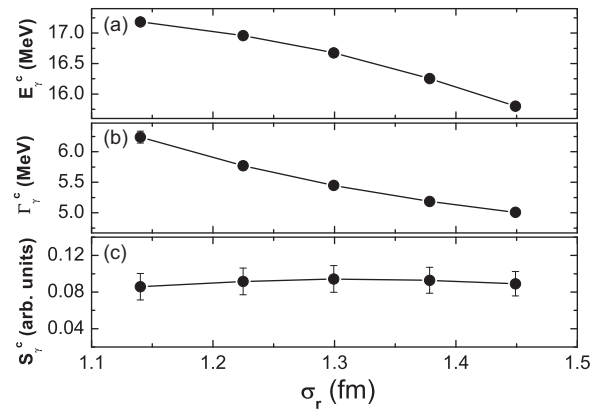


FIG. 8. Same as Fig. 3, but for  $\sigma_r$  dependence of GMR results for  $^{112}\text{Sn}$ . In the calculation, we use  $E_{\text{in}} = 386$  MeV/nucleon,  $b = 30$  fm,  $C_{\text{sym}} = 35.2$  MeV,  $\gamma = 1$ , and the soft EOS with MDI.

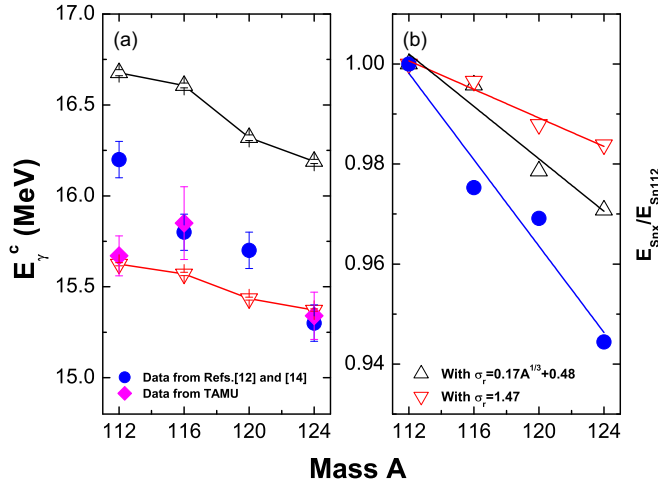


FIG. 9. (Color online) Mass-number dependence of the GMR peak energies for Sn isotopes with a fixed (down-triangles) or a mass-number dependent (up-triangle)  $\sigma_r$ . In the calculation, we use  $E_{in} = 386$  MeV/nucleon,  $b = 30$  fm,  $C_{sym} = 35.2$  MeV,  $\gamma = 1$ , and the soft EOS with MDI. In the left panel, the blue circles with error bar are the experimental data from Refs. [12,14], and the pink diamonds with error bar are the experimental data from Refs. [29,30]. In the right panel, the peak energies of GMR in Sn isotopes are divided by those in  $^{112}\text{Sn}$  to better illustrate the mass-number dependence, and the straight lines are plotted to guide the eyes.

the experimental data [12,29,30], respectively. One can see that the mass-number-dependent  $\sigma_r$  gives a larger peak energy and shows a stronger mass-number dependence of the GMR peak energy than the constant  $\sigma_r$ . However, it still gives a weaker mass-number dependence of the GMR peak energy in comparison with the experimental data as seen from the right panel of Fig. 9. Results from other theoretical studies [3,5] are also plotted for comparison. One can see that they overestimate the peak energies of GMR by about 0.3–1 MeV in Sn isotopes, and the mass-number dependence of the GMR peak energy seems also weaker than the experimental data.

### C. Fitting GMR peak energies with $\sigma_r$

From the above discussions, it is seen that introducing only the mass-number dependence to the width of the Gaussian wave packet for nucleons in the IQMD model is not sufficient to reproduce the experimental results of the GMR peak energies for Sn isotopes. However, considering the correlation between  $\sigma_r$  and the peak energy of GMR, we can fit the values of  $\sigma_r$  with the experimental data for different Sn isotopes. Figure 10 shows such a fit of  $\sigma_r$  for  $^{112}\text{Sn}$ ,  $^{116}\text{Sn}$ ,  $^{120}\text{Sn}$ , and  $^{124}\text{Sn}$  using the experimental results of GMR peak energies from Ref. [12]. It is seen that with the increasing mass and isospin asymmetry along the Sn isotope line, the GMR peak energy decreases while  $\sigma_r$  from fitting the GMR peak energy increases.

The above study gives us some hints that to reproduce reasonably well the experimental data of the GMR peak energies for Sn isotopes,  $\sigma_r$  may depend not only on the mass number but also on the isospin asymmetry of the nucleus.

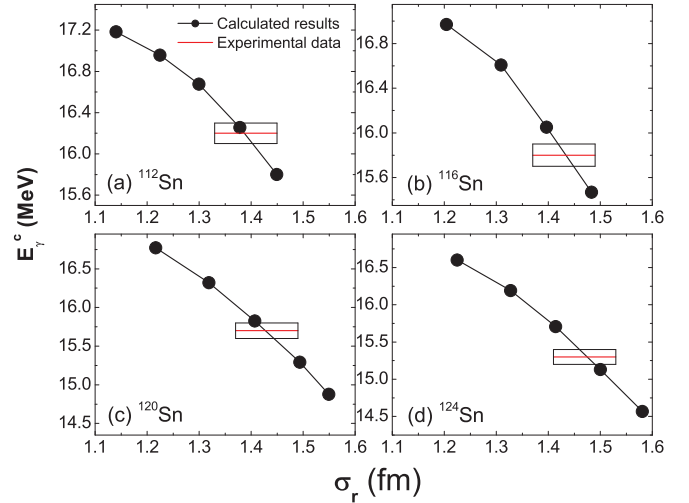


FIG. 10. (Color online) Fit of  $\sigma_r$  by the peak energies of GMR in  $^{112}\text{Sn}$ ,  $^{116}\text{Sn}$ ,  $^{120}\text{Sn}$ , and  $^{124}\text{Sn}$ . In the calculation, we use  $E_{in} = 386$  MeV/nucleon,  $b = 30$  fm,  $C_{sym} = 35.2$  MeV,  $\gamma = 1$ , and the soft EOS with MDI. The red line with the black rectangle representing the error is the experimental data from Ref. [12].

On the other hand, since the GMR peak energy is strongly correlated with the nucleus incompressibility  $K_A$  [12], it is reasonable to assume that  $\sigma_r$  has a functional form similar to that of  $K_A$ , i.e.,

$$\sigma_r = aA^{-1/3} + b[(N - Z)/A]^2 + cZ^2A^{-4/3} + d. \quad (21)$$

By fitting the experimental data of the GMR peak energies for Sn isotopes [12] with the above functional form, we obtain the following expression for  $\sigma_r$ :

$$\sigma_r = -3A^{-1/3} + 2.5[(N - Z)/A]^2 + 1.6 \times 10^{-8}Z^2A^{-4/3} + 2.01(\text{fm}). \quad (22)$$

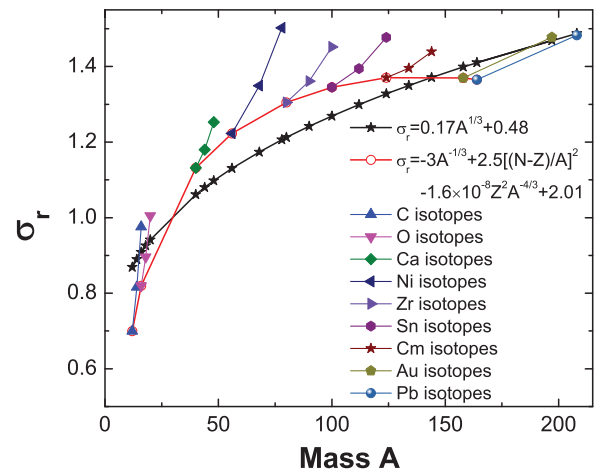


FIG. 11. (Color online) Mass-number dependence of the new function of  $\sigma_r$  given by Eq. (22) compared with that given by Eq. (20). The black line is the mass-number dependence given by Eq. (20). The red line is the one given by Eq. (22) for symmetric nuclei, and other lines are given by Eq. (22) for each isotopic chain.

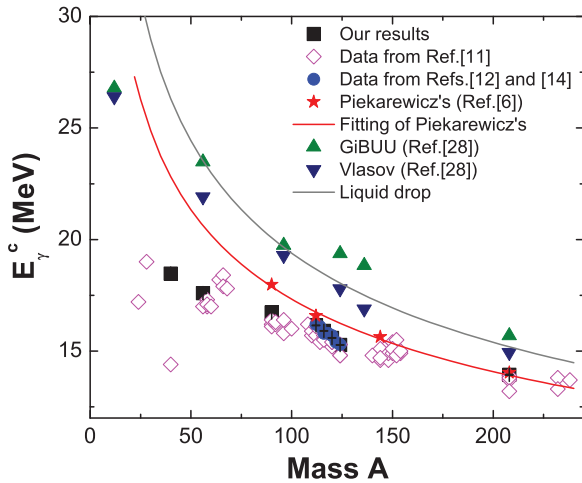


FIG. 12. (Color online) Mass-number dependence of the peak energy of GMR with  $\sigma_r$  given by Eq. (22). The blue circles with error bars are the experimental data from Refs. [12,14], and the open diamonds with error bars are the experimental data from Ref. [11] and references therein. The red line is a fitting of Piekarewicz's [6] results with  $E_\gamma^c = 69A^{-0.3}$  (MeV), and the gray line is a liquid drop fitting with  $E_\gamma^c = 90A^{-1/3}$  (MeV). In the calculation, we use  $E_{in} = 386$  MeV/nucleon,  $b = 30$  fm,  $C_{sym} = 35.2$  MeV,  $\gamma = 1$ , and the soft EOS with MDI.

The small coefficient for the charge-number dependence indicates that the optimized choice of  $\sigma_r$  might be a quadratic function of the nucleus isospin asymmetry. The new function of  $\sigma_r$  is compared with the old one [Eq. (20)] used in the QMD model in Fig. 11, and it is seen that they are quite different especially for isotope chains.

Equation (22) has also been extended in the calculation of GMR peak energies for  $^{40}\text{Ca}$ ,  $^{56}\text{Ni}$ , and  $^{90}\text{Zr}$  as well as  $^{208}\text{Pb}$  and the overall results are compared with those from other theoretical models [6,28] as well as the experimental data [11,12] in Fig. 12. It is found that after introducing the isospin dependence to the Gaussian wave-packet width fitted by the GMR peak energies for Sn isotopes of intermediate nucleus mass, our results agree with the experimental data for light or heavy nuclei such as  $^{56}\text{Ni}$  and  $^{90}\text{Zr}$  as well as  $^{208}\text{Pb}$  much better than others in the literature, which overestimate the GMR peak energies. For the even lighter nuclei such as  $^{40}\text{Ca}$ , although our result follows the same trend of mass-number dependence for intermediate and heavy nuclei, it overestimates the GMR peak energy compared with the experimental data. Different from the cases of intermediate and heavy nuclei, the GMR peak energies from the experimental studies fluctuate with mass number for light nuclei. This is due to the increasing effect of the shell structure as well as the pairing correlation for smaller nuclei, which has already been beyond the limit of the framework of the IQMD model and the other transport models with only mean-field potentials.

#### IV. SUMMARY

In this work, we have applied the IQMD model to investigate the isoscalar giant monopole resonance (GMR) in Sn isotopes and other nuclei. The collective oscillation, including the GMR mode, appears for an initial density distribution for the concerned nucleus, because it is generally not the ground state for the nuclear interaction used. This oscillation is further modified by the Coulomb interaction when we take the concerned nucleus as the projectile and the  $^{208}\text{Pb}$  nucleus as the target. We took the rms radius of the concerned nucleus as the monopole moment of GMR and calculated the spectrum of GMR. Using a Gaussian fit to the spectrum, we calculated the peak energy, the FWHM, and the strength of GMR. The sensitivity of these GMR results to the parameters used in the IQMD model was discussed. The GMR peak energy is found to slightly decrease with increasing incident energy, while it is almost independent of the impact parameter. It seems difficult to extract the information of the symmetry energy from the present study of GMR, because we found that GMR is also sensitive to other parameters such as the isoscalar part of the EOS and the Gaussian wave-packet width  $\sigma_r$ . As observed previously, the EOS associated with the nuclear incompressibility has an important influence on GMR. Comparing our results with the experimental data, it is found that the soft EOS with MDI can give a better fit to the experimental data. The studies of the systematic evolution for Sn isotopes have shown that a widely used mass-number-dependent  $\sigma_r$  overestimates the peak energies of GMR by about 1 MeV for Sn isotopes and leads to a weaker mass-number dependence of the GMR peak energies compared with the experimental data. By fitting the experimental data of the GMR peak energies for Sn isotopes using the functional form of the nucleus incompressibility, we obtain a new function of  $\sigma_r$  with isospin dependence in addition to mass-number dependence. Applying this new form of  $\sigma_r$  to the calculation of the GMR peak energies leads to a good agreement with the experimental data for  $^{56}\text{Ni}$ ,  $^{90}\text{Zr}$ , and  $^{208}\text{Pb}$ , although it still overestimates the GMR peak energy of  $^{40}\text{Ca}$  due to the lack of effects from shell structure as well as the pairing correlation in the IQMD framework. It will be interesting to check whether the width of the Gaussian wave packet for nucleons obtained from the present study can give better explanations for other observables from IQMD model calculations in future studies.

#### ACKNOWLEDGMENTS

This work was supported in part by the National Natural Science Foundation of China under Contracts No. 11035009, No. 11220101005, No. 10979074, No. 11175231, and No. 11205230; the Major State Basic Research Development Program in China under Contract No. 2013CB834405; the Knowledge Innovation Project of Chinese Academy of Sciences under Grant No. KJCX2-EW-N01; and the "100-Talent Plan" of Shanghai Institute of Applied Physics under Grant No. Y290061011 from the Chinese Academy of Sciences.

- [1] O. Civitarese, A. G. Dumrauf, M. Reboiro, P. Ring, and M. M. Sharma, *Phys. Rev. C* **43**, 2622 (1991).
- [2] B. K. Agrawal, S. Shlomo, and V. Kim Au, *Phys. Rev. C* **68**, 031304 (2003).
- [3] G. Colo, N. V. Giai, J. Meyer, K. Bennaceur, and P. Bonche, *Phys. Rev. C* **70**, 024307 (2004).
- [4] B. G. Todd-Rutel and J. Piekarewicz, *Phys. Rev. Lett.* **95**, 122501 (2005).
- [5] J. Piekarewicz, *Phys. Rev. C* **76**, 031301(R) (2007).
- [6] J. Piekarewicz and M. Centelles, *Phys. Rev. C* **79**, 054311 (2009).
- [7] V. Tselyaev *et al.*, *Phys. Rev. C* **79**, 034309 (2009).
- [8] E. Khan, *Phys. Rev. C* **80**, 011307 (2009).
- [9] E. Khan, *Phys. Rev. C* **80**, 057302 (2009).
- [10] E. Khan, J. Margueron, and I. Vidaña, *Phys. Rev. Lett.* **109**, 092501 (2012).
- [11] S. Shlomo and D. H. Youngblood, *Phys. Rev. C* **47**, 529 (1993), and references therein.
- [12] T. Li *et al.*, *Phys. Rev. Lett.* **99**, 162503 (2007).
- [13] U. Garg *et al.*, *Nucl. Phys. A* **788**, 36 (2007).
- [14] T. Li *et al.*, *Phys. Rev. C* **81**, 034309 (2010).
- [15] U. Garg, *Acta Phys. Pol. B* **42**, 659 (2011).
- [16] J. Blaizot *et al.*, *Nucl. Phys. A* **591**, 435 (1995).
- [17] D. Patel *et al.*, *Phys. Lett. B* **718**, 447 (2012).
- [18] H. L. Wu *et al.*, *Phys. Rev. C* **81**, 047602 (2010).
- [19] C. Tao, Y. G. Ma, G. Q. Zhang, X. G. Cao, D. Q. Fang, and H. W. Wang, *Phys. Rev. C* **87**, 014621 (2013); *Nucl. Sci. Tech.* **24**, 030502 (2013).
- [20] J. Aichelin, *Phys. Rep.* **202**, 233 (1991).
- [21] C. Hartnack *et al.*, *Eur. Phys. J. A* **1**, 151 (1998).
- [22] C. Hartnack *et al.*, *Nucl. Phys. A* **495**, 303c (1989).
- [23] Y. G. Ma *et al.*, *Phys. Rev. C* **73**, 014604 (2006).
- [24] Sanjeev Kumar, Suneel Kumar, and R. K. Puri, *Phys. Rev. C* **81**, 014601 (2010); **81**, 014611 (2010); S. Gautam and R. K. Puri, *ibid.* **85**, 067601 (2012).
- [25] G. Q. Zhang *et al.*, *Phys. Rev. C* **84**, 034612 (2011).
- [26] J. Wang *et al.*, *Nucl. Sci. Tech.* **24**, 030501 (2013).
- [27] V. Baran *et al.*, *Nucl. Phys. A* **679**, 373 (2001).
- [28] T. Gaitanos, A. B. Larionov, H. Lenske, and U. Mosel, *Phys. Rev. C* **81**, 054316 (2010).
- [29] D. H. Youngblood, Y. W. Lui, H. L. Clark, B. John, Y. Tokimoto, and X. Chen, *Phys. Rev. C* **69**, 034315 (2004).
- [30] Y. W. Lui, D. H. Youngblood, Y. Tokimoto, H. L. Clark, and B. John, *Phys. Rev. C* **70**, 014307 (2004).
- [31] B. A. Li, *Phys. Rev. Lett.* **85**, 4221 (2000).
- [32] W. J. Xie and F. S. Zhang, *Nucl. Sci. Tech.* **24**, 050502 (2013); W. Z. Jiang, *ibid.* **24**, 050507 (2013); C. W. Ma *et al.*, *ibid.* **24**, 050510 (2013).
- [33] S. Stringari, *Phys. Lett. B* **108**, 232 (1982).
- [34] L. W. Chen, B. J. Cai, C. M. Ko, B. A. Li, C. Shen, and J. Xu, *Phys. Rev. C* **80**, 014322 (2009).
- [35] T. Furuta, K. H. O. Hasnaoui, F. Gulminelli, C. Leclercq, and A. Ono, *Phys. Rev. C* **82**, 034307 (2010).
- [36] S. Gautam *et al.*, *J. Phys. G* **37**, 085102 (2010).
- [37] T. Maruyama, K. Niita, and A. Iwamoto, *Phys. Rev. C* **53**, 297 (1996).
- [38] H. Feldmeier, *Nucl. Phys. A* **515**, 147 (1990).
- [39] H. Feldmeier, K. Bieler, and J. Schnack, *Nucl. Phys. A* **586**, 493 (1995).
- [40] N. Wang, Z. X. Li, and X. Z. Wu, *Phys. Rev. C* **65**, 064608 (2002).